Title: The fate of carbon in a mature forest under carbon dioxide enrichment

M. Jiang[1], B.E. Medlyn[1], J.E. Drake[1,2], R.A. Duursma[1], I.C. Anderson[1], C.V.M. Barton[1], M.M. Boer[1], Y. Carrillo[1], L.Castañeda-Gómez[1], L. Collins[1,3,4], K.Y. Crous[1], M.G. De Kauwe[5], K.M. Emmerson[6], S.L. Facey[1,7], A.N. Gherlenda[1], T.E. Gimeno[1,8,9], S. Hasegawa[1,10], S.N. Johnson[1], C.A. Macdonald[1], K. Mahmud[1], B.D. Moore[1], L. Nazaries[1], U.N. Nielsen[1], N.J. Noh[1], R. Ochoa-Hueso[1,11], V.S. Pathare[1,12], E. Pendall[1], J. Pineiro[1], J.R. Powell[1], S.A. Power[1], P.B. Reich[1,13], A.A. Renchon[1], M. Riegler[1], P. Rymer[1], R.L. Salomón[14], B.K. Singh[1,15], B. Smith[1,16], M.G. Tjoelker[1], J.K.M. Walker[1], A. Wujeska-Klause[1], J. Yang[1], S. Zaehle[17], and D.S. Ellsworth[1]

Affiliation:

[1]Hawkesbury Institute for the Environment, Western Sydney University, Locked Bag 1797, Penrith, NSW, 2751, Australia

[2]Department of Forest and Natural Resources Management, College of Environmental Science and Forestry, State University of New York, Syracuse, NY 13210, USA.

[3]Department of Ecology, Environment and Evolution, La Trobe University, Bundoora, VIC 3086, Australia

[4]Arthur Rylah Institute for Environmental Research, Department of Environment, Land, Water and Planning, PO Box 137, Heidelberg, VIC 3084, Australia

[5]ARC Centre of Excellence for Climate Extremes, University of New South Wales, Sydney, NSW 2052, Australia

[6]Climate Science Centre, CSIRO Oceans & Atmosphere, Aspendale. VIC 3195, Australia.

[7]Department of Ecology, Swedish University of Agricultural Sciences (SLU), Uppsala, 75007, Sweden.

[8]Basque Centre for Climate Change, Leioa, 48940, Spain.

[9]Ikerbasque, Basque Foundation for Science, 48008 Bilbao, Spain.

[10]Department of Forest Ecology and Management, Swedish University of Agricultural Sciences (SLU), Umeå, SE-90183, Sweden.

[11]Department of Biology, IVAGRO, University of Cádiz, Campus de Excelencia Internacional Agroalimentario (CeiA3), Campus del Rio San Pedro, 11510 Puerto Real, Cádiz, Spain

[12]School of Biological Sciences, Post Office Box 646340, Washington State University, Pullman, WA 99164-6340, USA

[13]Department of Forest Resources, University of Minnesota, St Paul, Minnesota, 55108, USA

[14]Laboratory of Plant Ecology, Faculty of Bioscience Engineering, Ghent University, Coupure links 653, 9000 Ghent, Belgium.

[15]Global Centre for Land Based Innovation, Western Sydney University, Building L9, Locked Bag 1797, Penrith South, NSW, 2751, Australia

[16]Department of Physical Geography and Ecosystem Science, Lund University, 22362, Lund, Sweden

[17]Max Planck Institute for Biogeochemistry, Hans-Knöll-Str. 10, 07745 Jena, Germany

Abstract

Atmospheric carbon dioxide enrichment (eCO_2) can enhance plant carbon uptake and growth[1,2,3,4,5], thereby providing an important negative feedback to climate change by slowing the rate of increase of the atmospheric CO_2 concentration[6]. While evidence gathered from young aggrading forests has generally indicated a strong CO_2 fertilization effect on biomass growth[3,4,5], it is unclear whether mature forests respond to eCO_2 in a similar way. In mature trees and forest stands[7,8,9,10], photosynthetic uptake has been found to increase under eCO_2 without any apparent accompanying growth response, leaving an open question about the fate of additional carbon fixed under eCO_2[4,5,7,8,9,10,11]. Here, using data from the first ecosystem-scale Free-Air CO_2 Enrichment (FACE) experiment in a mature forest, we constructed a comprehensive ecosystem carbon budget to track the fate of carbon as the forest responds to four years of eCO_2 exposure. We show that, although the eCO_2 treatment of ambient +150 ppm (+38%) induced a 12% (+247 $gCm^{-2}yr^{-1}$) increase in carbon uptake through gross primary production, this additional carbon uptake did not lead to increased carbon sequestration at the ecosystem level. Instead, the majority of the extra carbon was emitted back into the atmosphere via several respiratory fluxes, with increased soil respiration alone contributing ~50% of the total uptake surplus. Our results call into question the predominant thinking that the capacity of forests to act as carbon sinks will be generally enhanced under eCO_2, and challenge the efficacy of climate mitigation strategies that rely on CO_2 fertilization as a driver of increased carbon sinks in standing forests and afforestation projects.

Main text

Globally, forests act as a large carbon sink, absorbing ~30% of total anthropogenic CO_2 emissions[1,12], an ecosystem service that has tremendous social and economic value. Whether

mature forests will remain carbon sinks into the future is of critical importance for aspirations to limit climate warming to no more than 1.5 °C above pre-industrial levels[13]. Free-Air CO_2 Enrichment (FACE) experiments provide an opportunity to determine the capacity of ecosystems to sequester carbon under the higher atmospheric CO_2 concentrations expected in the future[3,4,5,7,8,10,11]. Evidence gathered from the four first generation forest FACE experiments, which all measured responses of rapidly-growing young forest plantations, has generally indicated a strong CO_2 fertilization effect on biomass growth[3,4]. This CO_2 fertilization effect has been hypothesized to be one of the largest drivers of the terrestrial carbon sink and its acceleration in recent decades[14], potentially accounting for up to 60% of present-day terrestrial carbon sequestration[2]. Given that younger trees are generally more responsive to rising CO_2 than mature trees[11], extrapolating evidence collected from these experiments may be argued to provide an upper limit on how much carbon can be stored by global forests under eCO_2[15]. However, evidence from experiments with older trees suggests that although eCO_2 increases leaf photosynthesis to a similar degree as in young forests, stimulation of biomass growth and carbon storage may be lower or absent[7,8,9,10]. Reconciling these conflicting observations is a crucial step towards quantifying the carbon sequestration capacity of mature forests in the future. It requires that we identify the fate of the extra carbon fixed under eCO_2 in these complex ecosystems, which are expected to be closer to a state of equilibrium between carbon uptake and turnover, compared to young growing stands.

The *Eucalyptus* FACE (EucFACE) experiment is the world's first replicated, ecosystem-scale mature forest FACE experiment (Extended Data Figure 1). It is established in a warm-temperate evergreen forest that has remained undisturbed for the past 90 years and that is dominated by regionally widespread tree *Eucalyptus tereticornis*. The site is characterized by soils of low fertility with an understorey dominated by native grasses and shrubs. Seven

ecosystem-scale models were used to predict the eCO_2 response at EucFACE in advance of the experiment[16], highlighting three alternative hypotheses for the expected ecosystem response based on plausible assumptions incorporated in different models[17]. These hypotheses were: (i) enhanced photosynthesis under eCO_2 would lead to increased biomass accumulation; (ii) eCO_2-induced increase in photosynthesis would be directly down-regulated by limited nutrient availability; or (iii) eCO_2-induced increase in photosynthesis would lead to increased autotrophic respiration[16]. This range of predictions among a suite of well-tested models indicated a prognostic knowledge gap as to how the carbon cycling of mature forests would respond to the expected rise in CO_2 concentration[11], which is crucial to resolve in the face of future carbon-climate uncertainty[18].

To date, both canopy trees and understorey plants at EucFACE have shown increased rates of leaf photosynthesis but the canopy trees showed no significant increase in aboveground biomass growth under eCO_2[7], reflecting a similar lack of response observed in other eCO_2 experiments on mature trees[8,9,10]. Incorporating leaf-scale gas exchange measurements into a process-based tree stand model, it was estimated that the observed +19% stimulation of light-saturated overstorey leaf photosynthesis[7] corresponded to a +12% stimulation of whole-canopy gross primary production (GPP) response to eCO_2[19]. However, the probable fate of the extra carbon fixed under eCO_2 remained undetermined. Where did the extra carbon go?

To answer this question, we compiled measurements on all major carbon pools and fluxes collected over four years of experimental treatment (2013-2016), including individual and aggregated biomass and associated fluxes measured or inferred from plants, litter, soil, microbes, and insects, and constructed an ecosystem carbon budget (Figure 1) under both ambient (aCO_2) and eCO_2 conditions (+150 ppm). We first confirmed mass balance of the

ecosystem carbon budget by checking agreement between independent estimates of GPP and soil respiration (R_{soil}) derived from separate data streams (Extended Data Figure 2; see Methods). For GPP of the aCO_2 plots, we confirmed that a process-based model estimate of overstorey and understorey GPP (2059 ± 211 $gCm^{-2}yr^{-1}$), driven by site-specific meteorology and physiological data, agreed with the sum of data-driven estimates of net primary production (NPP) and autotrophic respiration (1968 ± 80 $gCm^{-2}yr^{-1}$). The carbon-use efficiency (NPP/GPP) of this mature forest was estimated to be 0.29 ± 0.02, which is on the low end of global forest estimates, but consistent with studies that have found this ratio tends to decline with stand age[20]. We further confirmed carbon mass balance for R_{soil} of the aCO_2 plots by comparing soil chamber-based estimates (1097 ± 86 $gCm^{-2}yr^{-1}$) with the sum of litterfall and independently estimated root respiration (1036 ± 27 $gCm^{-2}yr^{-1}$), assuming no change in soil carbon pool (see Methods). This agreement between independent estimates of components of the ecosystem carbon budget gives confidence that our measurements captured the pools and fluxes of carbon with low aggregate uncertainty and hence allows us to infer the fate of the extra carbon fixed under eCO_2.

To accommodate the inherent pre-treatment plot differences (see Methods), we normalized the CO_2 responses across plots by using a linear mixed-model with plot-specific pre-treatment leaf area index as a covariate[21,22]. The un-normalized eCO_2 responses are provided in Extended Data Figure 3, and generally confirm the findings but with less statistical precision. Our normalized responses (Figure 2, Extended Data Figure 4) showed that eCO_2 induced an average of 12% increase (+247 ± 195 $gCm^{-2}yr^{-1}$, mean ± one standard deviation) in carbon uptake, including contributions of overstorey (+192 ± 157 $gCm^{-2}yr^{-1}$) and understorey GPP (+55 ± 17 $gCm^{-2}yr^{-1}$). The fate of this additional carbon entering the system under eCO_2 was primarily traced to an increase in R_{soil} (+128.8 ± 95.2 $gCm^{-2}yr^{-1}$, or 52% of the carbon uptake surplus),

followed by a smaller increase in stem respiration (R_{stem}; +50.2 ± 47.2 $gCm^{-2}yr^{-1}$, or 20% of the carbon uptake surplus). In comparison, the increase in total NPP (+54 ± 12.9 $gCm^{-2}yr^{-1}$, or 22% of the carbon uptake surplus) was similar in magnitude to the increase in R_{stem}, but the increase in storage of the total carbon pools at the ecosystem-level was much smaller (ΔC_{pools}; +22.3 ± 176.4 $gCm^{-2}yr^{-1}$, or 9% of the carbon uptake surplus). There was thus little evidence of additional carbon accumulation under eCO_2 in this mature forest ecosystem. We then compared three alternative methods (see Methods) of estimating net ecosystem production (NEP; Figure 3). All three indicated that the ecosystem remained close to carbon-neutral under ambient CO_2 over the experimental period (mean ± SD for the methods: 74 ± 258, -35 ± 142, 115 ± 96 $gCm^{-2}yr^{-1}$, respectively), and that eCO_2 of +150 ppm did not result in statistically significant increases in ecosystem carbon storage (149 ± 261, -92 ± 216, 137 ± 230 $gCm^{-2}yr^{-1}$, respectively).

The relatively small but positive NPP response to eCO_2 was mainly driven by the understorey aboveground NPP response (NPP_{ua}; +50.3 ± 14.6 $gCm^{-2}yr^{-1}$), which was 93% of the net NPP response (Figure 2). However, this significant NPP_{ua} response did not result in an equivalent eCO_2 effect on understorey aboveground biomass increment (+27.2 ± 24.2 $gCm^{-2}yr^{-1}$), suggesting a possible higher understorey biomass turnover under eCO_2. Smaller fluxes, often neglected in other ecosystem carbon budgets, such as leaf consumption by insect herbivores (NPP_{ins}; 25.5 ± 4.3 vs. 27.8 ± 6.3 $gCm^{-2}yr^{-1}$, aCO_2 vs. eCO_2 mean ± SD), insect frass production (Frass; 10.5 ± 1.8 vs. 11.4 ± 2.6 $gCm^{-2}yr^{-1}$), vegetation volatile carbon emission (VC; 5.0 ± 0.12 vs. 4.3 ± 0.07 $gCm^{-2}yr^{-1}$), net ecosystem methane uptake (CH_4; 0.17 ± 0.04 vs. 0.17 ± 0.04 $gCm^{-2}yr^{-1}$), and leaching of dissolved organic carbon (DOC; 0.16 ± 0.02 vs. 0.17 ± 0.02 $gCm^{-2}yr^{-1}$), contributed to the closure of the overall ecosystem carbon budget (Figure 1; Extended

Data Figure 2), but were not important in explaining pathways of the carbon uptake surplus under eCO_2 (Figure 2, Extended Data Figure 4).

Here we provide some of the first replicated experimental evidence on the probable fate of carbon under eCO_2 in intact mature forests. We found that increased R_{soil} accounted for ~50% of the extra photosynthate produced by plants under eCO_2. It has been suggested that the increase in R_{soil} at EucFACE was likely a consequence of increased root and rhizosphere respiration[23,24], in contrast to other FACE sites where increased R_{soil} was attributed to enhanced soil organic matter decomposition (e.g. DukeFACE[25]). Here, the eCO_2-induced increase in R_{soil} was not accompanied by substantial changes in pools of fine root (+7.9 ± 8.4 $gCm^{-2}yr^{-1}$), microbial (+2.5 ± 2.9 $gCm^{-2}yr^{-1}$), mycorrhizal (+0.5 ± 0.4 $gCm^{-2}yr^{-1}$), leaf litter (-1.7 ± 6.2 $gCm^{-2}yr^{-1}$) or soil carbon (-23.8 ± 130.3 $gCm^{-2}yr^{-1}$), suggesting that the additional carbon fixed under eCO_2 may have led to an enhanced carbon transport belowground and a rapid belowground turnover of this flux. An initial enhancement in nitrogen and phosphorus mineralization was observed[26], which suggested that the increased R_{soil} with eCO_2 could reflect soil organic matter priming with the potential to alleviate plant nutrient stress in this phosphorus-deprived environment[26,27]. However, the enhanced soil mineralization rate and associated increase in nutrient availability did not persist over time[26], indicating that this increased belowground carbon allocation and the rapid turnover of this flux was not effective in increasing phosphorus availability to the plants[7,28].

The ecosystem carbon budget presented here provides an opportunity to confront the three alternative hypotheses of the response of this system to eCO_2 treatment that emerged from model predictions made in advance of the experiment[16]. Our data do not support any of the three hypotheses. The eCO_2-induced increase in photosynthesis was not strongly down-

189 regulated by low nutrient availability; nor did the eCO_2-induced additional carbon uptake lead
190 to additional biomass accumulation, or enhanced aboveground respiration[16]. These predictions
191 reflect common mechanisms by which terrestrial vegetation models implement nutrient
192 limitation of the eCO_2 response[16,17,29,30]. In contrast, our results suggest a direct connection
193 between plant photosynthesis and belowground activity, in which increased belowground
194 carbon allocation increased soil respiration at a rate that accounted for half of the extra carbon
195 fixed under eCO_2. This increased soil respiration has been demonstrated by some models to be
196 an important and often overlooked mechanism that reduces global soil carbon sequestration
197 relative to estimates by many current models[31]. As a consequence of including this rapid
198 turnover of the increased belowground carbon allocation in terrestrial biosphere models, the
199 time lag in emitting some of the extra carbon via biomass accumulation and litterfall input into
200 the soils may be reduced, thereby leading to faster cycling of carbon[32] and therefore possible
201 different trajectories of carbon-climate predictions for the future.
202
203 A major form of land-based climate mitigation actions envisaged in the Paris Agreement is to
204 enhance forest biomass carbon stocks globally through the protection of existing, largely
205 mature, forests, and through afforestation of new areas. The mitigation potential of forests lies
206 in the accumulated stock of ecosystem carbon, not in the short-term rate of forest
207 photosynthesis. The probable fate of additional carbon determined in our study (Figure 2)
208 challenges the current thinking that non-aggrading mature forests can contribute to enhanced
209 carbon sinks due to CO_2 fertilization[33], which further questions the allowable CO_2 emission
210 targets sourced from existing carbon cycle models[13,34]. Given that the effect of CO_2 fertilization
211 may be one of diminishing returns over time[14], the statistically insignificant eCO_2 effect on
212 NEP (Figure 3), if representative of mature forest ecosystems generally, suggests an even
213 weaker carbon sink in the future, especially in low fertility systems such as EucFACE. Future

214 research efforts should target a deeper understanding of the nutrient-carbon feedbacks that
215 likely constrain the carbon sink potential of mature forests under eCO_2, and evaluate the
216 implications of a potentially weaker terrestrial land carbon sink in the development of robust
217 mitigation strategies in the face of climate change.
218

Methods

EucFACE site description

The EucFACE facility (Extended Data Figure 1) is located in a mature evergreen *Eucalyptus* forest on an alluvial spodosol in western Sydney, Australia (33°36'S, 150°44'E). The site has been a remnant patch of native Cumberland Plain woodland since the 1880's and has remained unmanaged for at least the past 90 years, with *Eucalyptus tereticornis* Sm. as the dominant tree species. *Eucalyptus* trees occur naturally across Australia, accounting for 78% of native forest area in Australia[35] and are planted widely around the globe[36]. Infrastructure for six large circular plots (490 m^2 each) was established in 2010. Starting on 18th September 2012, three plots were subjected to free-air CO_2 enrichment treatment using computer-controlled pre-dilution method. The CO_2 concentrations at EucFACE were ramped up over a six-month period, increasing by +30 ppm every five weeks in discrete steps (+30, 60, 90, 120, and 150 ppm). The full elevated CO_2 treatment of +150 ppm started on 6th February 2013 during daylight hours over all days of the year. The site is characterized by a humid temperate-subtropical transitional climate with a mean annual temperature of 17.5°C and a mean annual precipitation of 800 mm (Figure S1). The soil is a Holocene alluvial soil of low-fertility with low phosphorus content[7,37]. Soil texture is a loamy sand (> 75% sand content) up to 50 cm in depth. From ca. 50 to 300 cm depth, soils are sandy clay loam, with > 30% silt and clay. Average bulk density is 1.39, 1.69 and 1.71 g cm^{-3} for depths of 0-10, 10-20 and 20-30 cm, respectively (Figure S2). Permanent groundwater depth is ~11 m below the soil surface[38]. Understorey vegetation is a diverse mixture of 86 species including forbs, graminoids and shrubs[39]. The dominant understorey species is *Microlaena stipoides*, a C3 perennial grass that accounted for ~70 % of herbaceous biomass, and responded rapidly to rainfall variability[40].

Estimates of carbon pools and fluxes

We estimated plot-specific carbon pools and fluxes at EucFACE over 2013-2016 (Extended Data Table 1). We defined pools as a carbon reservoir and annual increments as the annual change in the size of each reservoir. We compartmentalized the ecosystem into 10 carbon pools, namely overstorey leaf (C_{ol}), stem (C_{stem}), fine root (C_{froot}), coarse root (C_{croot}), understorey aboveground (C_{ua}), soil (C_{soil}), microbe (C_{micr}), mycorrhizae (C_{myco}), leaf litter (C_{lit}), and aboveground insect (C_{ins}) carbon pools, and reported pool size in the unit of gCm^{-2}. We defined fluxes as components of the carbon flow through the system, and report them in the unit of $gCm^{-2}yr^{-1}$. All annual incremental changes in carbon pools were reported in $gCm^{-2}yr^{-1}$ with a symbol Δ. We converted estimates of biomass into carbon content using variable-specific carbon fractions (f) defined in Extended Data Table 2. Below we describe how each pool and flux was estimated.

Pools

Soil carbon pool (C_{soil}; Figure S2**)** was estimated based on quarterly sampled soil carbon content (oven-dried at 40 °C for 48 hours) and plot-specific soil bulk density at three depths (0 - 10 cm, 10 - 20 cm, 20 - 30 cm). Out of the 15 dates when samples were taken, only 3 of these measured soil carbon content below the top 10 cm of soil. To obtain a more accurate estimate of annual incremental change in soil carbon pool, we therefore reported soil carbon pool for the top 10 cm only. There were no temporal and eCO_2 trends in soil carbon content at deeper depths.

Overstorey leaf carbon pool (C_{ol}; Figure S3**)** was estimated based on continuous measures of leaf area index (LAI) and specific leaf area (SLA), following C_{ol} = LAI x SLA x f_{ol}, where f_{ol}

267 is a carbon fraction constant for overstorey leaf (Extended Data Table 2). Daily averages of
268 plot-specific LAI were estimated based on the attenuation of diffuse radiation in a homogenous
269 canopy[22]. The number of observations varies between days, depending on the number of 30-
270 minute cloudy periods. SLA was estimated based on time-series measures of leaf mass per area
271 (LMA), and was then linearly interpolated to plot-specific daily values over time.
272
273 **Stem carbon pool (C_{stem};** Figure S4**)** was estimated based on tree-specific height and diameter
274 at breast height (DBH) measurements, and an allometric scaling relationship derived based on
275 *E. tereticornis*[7,41]. DBH changes were measured repeatedly at roughly one month intervals at
276 1.3 m height. Bark was periodically removed from under the dendrometer bands - this effect
277 on DBH was considered by calculating biomass once per year using December data only. Stem
278 biomass data were summed for each plot and averaged over the plot area to obtain ground-
279 based estimates, and was then converted into C_{stem} using treatment-specific carbon fraction
280 (Extended Data Table 2).
281
282 **Understorey aboveground carbon pool (C_{ua}**; Figure S5**)** was estimated at 1-3 month intervals
283 between February 2015 and December 2016 using non-destructive measurements of plant
284 height obtained from stereo-photography[42]. In each of the four 2m x 2m understorey
285 monitoring subplots within each plot, stereo photographs were collected using a Bumblebee
286 XB3 stereo camera (Point Grey Research) mounted ~2.4 m above the ground surface and facing
287 vertically downwards towards the center of the subplot. Stereo images were taken at dusk under
288 diffuse light conditions to avoid measurement errors related to shadows from trees and
289 EucFACE infrastructure. On each sampling date, three sets of stereo photographs were taken
290 in each subplot to produce large number (i.e. 100,000s) of understorey plant height estimates
291 from which mean plant height (H_{mean}, in m) was calculated for each plot. Understorey

aboveground biomass (B_{ua}, in kg m^{-2}) for each plot was predicted from H_{mean} using an empirical model developed for the grassy understorey vegetation at EucFACE (B_{ua} = 1.72 * H_{mean} – 0.05)[42]. The four subplot-level estimates were averaged to obtain a plot-level estimate of B_{ua}, and then converted to an estimate of C_{ua} using a carbon fraction constant (Extended Data Table 2).

Root carbon pool (C_{root}) consists of fineroot (C_{froot}) and coarseroot (C_{croot}) pools, with C_{froot} defined as roots with diameter < 2 mm, with the remaining roots or woody roots defined as C_{croot} (Figure S6). The C_{root} pool includes roots of both overstorey and understorey vegetation. Total root carbon pool (C_{root}) was estimated based on an allometric relationship between root biomass (B_{root}) and stand basal area (derived from DBH) derived for Australian forest species[43], as follows:

$$ln(B_{root}) = 0.787 * ln\ (DBH) + 1.218$$

Fineroot biomass was estimated based on standing biomass sampled at 4 subplots per plot at 2 depths (0 - 10 cm and 10 - 30 cm) over the period of 2014-2015[27]. Plot-specific fineroot biomass was taken by summing biomass data across depths. Coarseroot biomass was estimated as the net difference between fineroot and total root biomass. The fineroot and coarseroot biomass were multiplied by the corresponding carbon fraction constants to obtain C_{froot} and C_{croot}, respectively (Extended Data Table 2).

Microbial carbon pool (C_{micr}) was estimated based on fumigation extraction and 0.5 M K_2SO_4 extraction as in Ref. 23 using samples taken at 0-10 cm soil depth over the period of 2012 - 2015. Total organic carbon was determined on a Shimadzu TOC analyzer (TOC-L TNM-L; Shimadzu, Sydney, Australia), which was then multiplied by soil bulk density over the same soil depth to obtain the C_{micr} (Figure S7a).

317

318 **Mycorrhizal carbon pool (C_{myco})** for the top 10 cm of soil was estimated via measurements
319 of colonization of mycorrhizal in-growth bags, carbon isotopic partitioning, microbial
320 phospholipid fatty acid abundance and C_{micr}. Nine 45 µm nylon mesh bags (4 x 5 cm) filled
321 with sand, which excluded roots but allowed access of fungi[44], were buried in November 2014
322 in each experimental plot and three bags were subsequently collected every four months for
323 one year. Phospholipid-derived fatty acids (PLFA), a proxy for total microbial biomass
324 abundance, were quantified in sand bags and native field soil following the protocol by Ref.
325 45. $\delta^{13}C$ values of ground subsamples of this sand, native soil carbon, and aboveground plant
326 tissue (leaves of Eucalypts in April 2014) were used to estimate the fraction of the accumulated
327 carbon in sand bags that was derived from plant carbon using isotopic mass balance. Due to
328 the exclusion of roots, plant derived carbon in bags can be attributed to mycorrhiza. This plant-
329 derived unitless fraction was then multiplied by the total concentration of PLFA in sand bags
330 to obtain the amount of the total PLFA contributed by mycorrhiza (µg PLFA / g sand). To scale
331 this to native soil PLFA concentrations we then calculated the ratio between mycorrhizal PLFA
332 in sand bags to total PLFA in soil (representing the total microbial pool). Subsequently, to
333 estimate C_{myco}, this ratio was multiplied by the C_{micr} in each plot (Figure S7b).

334

335 **Leaflitter carbon pool (C_{lit})** was estimated based on leaf litter decomposition rate and leaf
336 litterfall data collected by litter baskets (Figure S8)[22]. Leaf litter decomposition rates were
337 estimated over 24 months using litter bags. Briefly, 2 g air-dried *Eucalyptus* litter was added
338 to 10 x 15 cm litter bags with a 2-mm mesh size. Twelve litter bags were randomly allocated
339 to 4 subplots within each treatment plot, and two litter bags were collected at 3, 6, 9, 12, 18
340 and 24 months to calculate mass loss over time (mass loss was averaged across the two
341 replicates from each subplot). A leaflitter exponential decay function was estimated for each

plot, based on data collected over this 24-month period. Leaf litterfall was estimated from monthly collections of material from circular fine-mesh traps (each 0.2 m^2) at 8 random locations for each plot. We then applied the exponential decay function with litterfall biomass to obtain C_{lit}, assuming a carbon fraction constant (Extended Data Table 2).

Insect carbon pool (C_{ins}) was estimated based on two different sampling techniques, with aerial insects partially estimated based on monthly dead insect data collected from circular fine-mesh traps of 0.2 m^2 at 8 random locations for each plot[46], and understory insects estimated based on vacuum suction sampling from 2 locations for each plot[47]. The vacuum suction method collected invertebrates from understorey vegetation in two 1 x 1 m subplots using a petrol-powered 'G-Vac' vacuum device run on full-throttle for 20 s, for a total of 5 sampling campaigns. Trapping locations were randomly chosen and fixed between sampling campaigns. All invertebrates were sorted from debris, dried to constant weight at 60°C and weighed on a microbalance with an accuracy of 1 μg. We assume that vacuum samples as well as litter trap samples represent point estimates of invertebrate abundance. Then, the total biomass of sampled invertebrates was summed across sampling methods within each plot. A constant carbon fraction based on Ref. 48 (Extended Data Table 2) was used to convert biomass into C_{ins} pool (Figure S9).

Ecosystem carbon uptake fluxes

Overstorey gross primary production (GPP_O) for each plot was provided by a stand-level model simulation (MAESTRA), forced by hourly meteorological data and interpolated photosynthetic parameters measured at the site (Figure S10a)[19]. In MAESTRA, each plot consists of individual tree crowns that are located and parameterized with measured coordinates, crown size, and LAI. Each crown was divided into six layers, with leaf area uniformly distributed into each layer. Within each layer, the model simulated twelve points.

367 The radiation at each grid point considered shading from upper crown and surrounding trees,
368 solar angle (zenith and azimuth), and light source (diffused or direct). According to the
369 radiation, the leaf area at each grid point was divided into sunlit and shaded leaves, which was
370 used to calculate gas exchange using a Farquhar[49] type formulation for photosynthesis.
371 Calculations for carbon flux were parameterized with *in situ* leaf gas exchange
372 measurements[7,50]. Respiration and its temperature dependence were also quantified using data
373 collected on site. The output was evaluated against measured canopy-scale transpiration data[19].
374
375 Similarly, **understorey GPP (GPP_u)** (Figure S10b) was simulated using MAESTRA with
376 photosynthetic parameters taken for the grass *Microlaena stipoides*[40]. The parameterization of
377 understory vegetation is different from that of the canopy. In each plot, the understory was
378 assumed to form a single crown covering the whole plot (i.e., a circle with 12.5 m radius) at a
379 height of 1.5 m. The LAI of the understory was estimated using phenology camera digital
380 photographs taken at four permanent understorey vegetation monitoring subplots in each plot[42].
381 The average green pixel content was calculated from three photos in each subplot, and assumed
382 to be the same as the fraction of absorbed PAR. We then assumed a light extinction coefficient
383 of 0.5 in Beers' Law and calculated understorey LAI. Before 2014 there were 3 campaigns per
384 year while from 2014 the cameras were automated, and we used the fortnightly averages. Leaf
385 gas exchange parameters were obtained from Ref. 40 and covered four to six campaigns per
386 year from 2013 to 2016. We estimated a one-time g_1 parameter[51] for all plots and time, and
387 assumed constant carboxylation rate (V_{cmax}) and electron transport rate (J_{max}) values at 25 ºC
388 across plots. Basal leaf respiration rate and the temperature dependence of photosynthesis and
389 respiration were assumed to be the same as the canopy. The understory simulation was
390 conducted separately from the canopy, with canopy LAI from Ref. 22 included to account for
391 the shading from the canopy, branches and stems on the understory.

For the **methane net flux (CH_4),** air samples were collected following the closed-chamber method (or Non-Flow-Through Non-Steady-State [NFT-NSS] method). Seven replicated chambers were available for each plot. Headspace samples were collected monthly, over a period of one hour and analyzed by gas chromatography. Fluxes were estimated by a mixture of linear and quadratic regressions (depending on goodness-of-fit), assuming a constant air pressure of one atm and correcting the air temperature inside the chambers for each air sample[52]. The CH_4 fluxes are net fluxes, which represent the sum of: 1) CH_4 efflux (emissions from the soil into the atmosphere); 2) CH_4 influx (uptake from the atmosphere into soil). Here, the annual net CH_4 flux was an ecosystem influx and was presented as positive values (Figure S11a).

Production fluxes

Plant **net primary production (NPP)** is the sum of overstorey leaf (NPP_{ol}), stem (NPP_{stem}), fine root (NPP_{froot}), coarse root (NPP_{croot}), other (including twigs, barks, and seeds; NPP_{other}), understorey aboveground (NPP_{ua}), and consumption of overstorey leaf by insect herbivores (NPP_{ins}). NPP_{ol} and NPP_{other} were estimated based on monthly litter data collected from circular fine-mesh traps of 0.2 m^2 at eight random locations for each plot (Figure S12). Litter were sorted into leaf, twigs, bark, and seeds, dried to constant mass at 40 °C and weighed. A subsample was reweighed when dried to constant mass at 70 °C and a small moisture correction was applied to the leaf component of the whole dataset. NPP_{ol} was computed as the sum of annual leaf litter, which excluded leaf consumption by insects. For twigs, we assumed strictly annual turnover across the years. NPP_{stem} (Figure S13) and NPP_{croot} (Figure S14) were estimated based on annual incremental change of stem biomass and coarse root biomass,

416 respectively. NPP_{froot} was estimated based on samples collected from the in-growth cores at 4
417 different locations per plot (Figure S14).
418
419 NPP_{ua} was estimated based on biomass clippings taken between 2015 - 2017, assuming one
420 understorey turnover per harvest interval (Figure S15). We used a clip-strip method of biomass
421 harvest as has been applied previously at the BioCON experiment[53]. Specifically, four narrow
422 strips, each with a size of 1 m x 0.1 m, were situated in each of the experimental plots at least
423 2 m away from the vertical pipes for FACE, while avoiding the understory shrubs. The
424 understory herbaceous species were clipped approximately 1 cm above soil level. The total
425 mass per harvest represents the total production. Biomass samples were oven dried for two
426 days at 60 ^{o}C, and converted into carbon mass by applying a constant fraction (Extended Data
427 Table 2).
428
429 NPP lost to overstorey leaf consumption by insect herbivores (NPP_{ins}) was estimated based on
430 insect frass data (Frass) collected from the circular fine-mesh traps, and a relationship between
431 frass mass and insect consumed leaf mass derived based on multiple *Eucalyptus* tree species at
432 different CO_2 concentrations (Figure S16a)[54,55]. Frass was estimated based on annual collection
433 of frass biomass collected from the circular fine-mesh litter traps with their associated carbon
434 content (Extended Data Table 2; Figure S16c).
435

436 *Outfluxes*

437 Leaching lost as **dissolved organic carbon (DOC)** from soils was estimated based on
438 concentrations of DOC in soil solutions, provided by water suction lysimeter measurements[26].
439 Lysimeters were installed to two depths (0 - 15 cm and 35 - 75 cm, which is immediately above
440 the impermeable layer). Here we assumed that DOC reaching deeper depth is lost from the

441 system at a rate of 20 ml m^{-2} d^{-1}, which is an estimate of the daily drainage rate at the site
442 (Figure S11b).
443
444 **Plant autotrophic respiration (R_a)** consists of overstorey leaf (R_{ol}), stem (R_{stem}), root (R_{root}),
445 understorey aboveground (R_{ua}) (Figure S17), and growth respiration (R_{grow}) (Figure S18). R_{ol}
446 and R_{ua} were based on MAESPA simulation (Figure S17a, c), as described in the respective
447 GPP sections. R_{grow} was estimated by taking a constant fraction of 30% of total NPP as
448 measured directly on *E. tereticornis* trees[56].
449
450 R_{stem} was estimated from measurements of stem CO_2 efflux performed in three dominant trees
451 per plot (Figure S17b). Collars were horizontally attached to the stem at an approximate height
452 of 0.75 m, and R_{stem} was measured with a portable infrared gas analyzer coupled to a soil
453 respiration chamber adapted for this purpose[57]. Measurement campaigns were performed every
454 one or two months from December 2017 to October 2018, and the relationship between R_{stem}
455 and air temperature (T_{air}) was used to extrapolate R_{stem} across the surveyed period, following
456 $R_{stem} = 0.1866 * 2.84^{Tair/10}$ ($r^2 = 0.42$, $p < 0.0001$). R_{stem} was then upscaled to the stand level
457 considering the ratio of trunk stem axial surface per unit of soil surface measured per plot. Stem
458 surface area was directly inferred from the Terrestrial Laser Scanning (TLS) data through
459 quantitative structure models presented in Ref. 58 and 59. TLS data were acquired with a
460 RIEGL VC-400 terrestrial laser scanner (RIEGL Laser Measurement Systems GmbH). Stem
461 surface area was derived from the TLS data following a two-step approach: (i) manually
462 extracting single tree from the registered TLS point cloud; and (ii) deriving parameters for an
463 extracted single tree. Once a tree is extracted from the point cloud, the next step was to strip
464 off the leaves, and segment the point cloud into stem and branches. Finally, the surface of the
465 segments was reconstructed with geometric primitives (cylinders). The method used a cover

466 set approach, where the point cloud was partitioned into small subsets, which correspond to
467 small connected patches in the tree surface.
468
469 R_{root} was partitioned into fineroot (R_{froot}) and coarse root (R_{croot}) respiration (Figure S17d). Both
470 R_{froot} and R_{croot} were estimated based on soil temperature at 20 cm depth. Mass-based rates of
471 R_{froot} were obtained from measured rates in seedlings of *E. tereticornis*[60]. R_{croot} was estimated
472 using a proxy based on measured rates of wood respiration of branches (c. 7 mm diameter) in
473 trees (8 to 9 m height) of *E. tereticornis*[61]. The equations are:

474 $$R_{froot} = B_{fr} * 4.425 * 2.26^{(Tsoil - 15)/10}$$

475 $$R_{croot} = B_{cr} * 1.33 * 2.26^{(Tsoil - 15)/10}$$

476 where R_{froot} and R_{croot} are fine root and coarse root respiration rates, respectively, T_{soil} is soil
477 temperature at 15 min interval, B_{fr} and B_{cr} are fineroot and coarse root biomass, respectively.
478 Here we assumed fraction of coarse root at top 30 cm of soil is 60 % to represent coarse root
479 respiration at this soil profile.
480
481 **Carbon efflux due to insect respiration (R_{ins})** was estimated as the net difference between
482 NPP_{ins} and Frass, assuming no net change in insect biomass (Figure S16b).
483
484 **Soil respiration (R_{soil}):** The rate of soil CO_2 efflux was measured at eight locations within each
485 plot, where a permanent PVC collar inserted into the soil was co-located with soil TDR probes
486 for continuous measurements of soil temperature (5-cm-depth) and volumetric water content
487 (0 to 21-cm-depth; CS650-L; Campbell Scientific, Logan, UT, USA). R_{soil} was measured
488 manually at all collar locations every 2-3 weeks, in addition to 30-minute measurements using
489 automated chambers (Li-8100-103; Licor) at one location within each plot, resulting
490 in >300,000 observations over the study period[24]. These data were used to parameterize a semi-

491 mechanistic model of R_{soil}, in which R_{soil} was predicted based on measurements of soil
492 properties, soil physics, and measured soil temperature and volumetric water content[62]. This
493 model successfully recreated the observed fluxes (r^2 between predicted and observed survey
494 R_{soil} was 0.65)[24]. Annual sums of R_{soil} were derived by summing the averaged daily fluxes over
495 eight locations within each plot, where daily fluxes at each location were predicted based on
496 the semi-mechanistic model and daily soil temperature and volumetric water content data taken
497 adjacent to each measurement collar. Soil heterotrophic respiration (R_{hetero}) was taken as the
498 net difference between R_{soil} and R_{root} (Figure S19). Total ecosystem respiration (R) was
499 calculated as the sum of R_a, R_{hetero}, R_{ins}, and VC.
500
501 **Volatile carbon (VC;** Figure S20**)** flux as isoprene (C_5H_8) was estimated using the Model of
502 Emissions of Gases and Aerosols from Nature (MEGAN)[63]. Isoprene represents over half of
503 all VOC species emitted by vegetation globally. A MEGAN box-model was built from the
504 version used in Ref. 64, centered on the EucFACE facility to calculate hourly emissions of
505 isoprene across the period 2013-2016 for all six plots:
506 $$VC = EF * LAI * \gamma$$
507 Where EF is the isoprene basal emission factor, γ is the emission activity factor, accounting for
508 changes in the isoprene response due to light, temperature, leaf age and soil moisture. The
509 MEGAN simulations were driven by daily input data of LAI, soil moisture, and hourly input
510 data of photosynthetic active radiation, temperature, atmospheric pressure, wind speed and
511 relative humidity. The isoprene EFs were measured as 6.708 mg m^{-2} h^{-1} for ambient CO_2 plots
512 and 5.704 mg m^{-2} h^{-1} for elevated plots. The EFs were derived from in-line photosynthetic gas-
513 exchange measurements coupled with simultaneous volatile isoprenoid sampling. The isoprene
514 emissions were collected in sterile stainless steel thermal desorption tubes at the same time as
515 gas exchange was measured, and these were capped and later thermally desorbed for off-line

volatile analysis in the laboratory using a Shimadzu GC/MS. The chromatographic peaks were identified by comparing them to isoprene standards and reference mass spectra in the NIST Mass Spectral Library (https://www.nist.gov/srd). The box-model produced isoprene was converted to carbon content using the molecular weight ratio of carbon to isoprene.

Net Ecosystem Production

Net ecosystem production (NEP) was estimated based on three different methods that estimated NEP in relatively independent ways (Figure 3), similar to Ref. 65. The first method considered NEP as the difference between total ecosystem influx and total ecosystem outflux (i.e. In - Out), which relied on both process-based modeling and empirical upscaling of respiratory fluxes collected from the field. The second method considered NEP as NPP minus R_{hetero} (i.e. NPP - R_{hetero}), with NPP relying mostly on litter-based production estimates, and R_{hetero} relying on R_{soil} and R_{root} estimates. The third method considers NEP as the sum of changes in carbon pools in the ecosystem (i.e. ΔC_{pools}), which was mostly determined by biomass estimates. Equations for each method are provided below:

Method	**NEP =**
In - Out	$GPP_o + GPP_u + CH_4 - R_{ol} - R_{stem} - R_{soil} - R_{ua} - R_{ins} - DOC - VC - R_{grow}$
NPP - R_{hetero}	$NPP_{ol} + NPP_{stem} + NPP_{froot} + NPP_{croot} + NPP_{other} + NPP_{ua} + NPP_{ins} - R_{hetero}$
ΔC_{pools}	$\Delta C_{soil}+\Delta C_{ol}+\Delta C_{stem}+\Delta C_{croot}+\Delta C_{froot}+\Delta C_{ua}+\Delta C_{lit}+\Delta C_{ins}+\Delta C_{micr}+\Delta C_{myco}$

Carbon budget evaluation

We evaluated the mass balance of our estimated ecosystem carbon budget in two ways. Firstly, we compared model simulated GPP with the aggregated sum of NPP and R_a (Extended Data Figure 2a, b). GPP was simulated by a stand-level ecophysiological model, driven by hourly

meteorological data and parameterized with site-specific ecological data[19]. This GPP should equal to the aggregation of NPP (NPP_{ol} + NPP_{stem} + NPP_{froot} + NPP_{croot} + NPP_{other} + NPP_{ua} + NPP_{ins}) and R_a fluxes (R_{ol} + R_{stem} + R_{root} + R_{ua} + R_{grow}), which were mostly extrapolated based on field data. Secondly, R_{soil} estimated based on soil collar flux measurements[23] was evaluated against the sum of litterfall and R_{root} (Extended Data Figure 2c, d), assuming minimal changes in soil carbon stock (as change over this short period of time is beyond the detection limit in a complex and slow-growing mature forest ecosystem like EucFACE). Here, litterfall was the sum of NPP_{ol} + NPP_{froot} + NPP_{croot} + NPP_{other} + NPP_{ua} + Frass, and R_{root} was extrapolated based on root biomass and temperature functions.

Statistical analyses

We performed linear mixed-model analysis using the "lmer" function within the "lme4" package[66] in software R[67] to determine the CO_2 treatment effect on all reported variables. All fluxes were reported at an annual rate ($gCm^{-2}yr^{-1}$). In our model, date and CO_2 treatment were considered as fixed factors, plot as a random factor, and plot-specific pre-treatment LAI (i.e. 4-month average LAI before full CO_2 treatment was switched on) as a covariate to account for pre-treatment differences among treatment plots. Normalizing all response variables with a covariate that integrates light, water and nutrient constraints helps to isolate the CO_2 effect[21], as has been done previously at the site[22] and elsewhere[8,21]. Confidence intervals for the CO_2 effect size of individual variables were reported using the function "confint", which applies quantile functions for the t-distribution after model fitting. Confidence intervals for the predicted flux and pool were reported as the standard deviation of the plot-specific totals (n = 3). Similarly, confidence intervals for the aggregated fluxes (e.g. NPP) were reported by summing individual component fluxes that constituent the aggregated flux for each plot and

computing the standard deviations across plots (n = 3). Finally, confidence intervals for the CO_2 effect size (SD_{agg}) of some aggregated fluxes (e.g. NPP) were calculated by pooling the standard deviations of the aggregated fluxes for ambient (SD_{amb}) and elevated CO_2 treatment (SD_{ele}), following:

$$SD_{agg} = \sqrt{\frac{SD_{amb}^2 + SD_{ele}^2}{2}}$$

Data statement

Data and code will be made available via Research Data Australia upon acceptance of the manuscript.

References

1. Le Quéré C.L. *et al*. Global carbon budget 2018. *Earth Syst. Sci. Data* **10**, 2141-2194 (2018).
2. Schimel D. *et al.* Effect of increasing CO_2 on the terrestrial carbon cycle. *Proc. Natl. Acad. Sci. USA* **112**, 436-441 (2015).
3. Walker A.P. *et al*. Decadal biomass increment in early secondary successional woody ecosystems is increased by CO_2 enrichment. *Nat. Commun.* **10**, 454, https://doi.org/10.1038/s41467-019-08348-1 (2019).
4. Norby R.J. & Zak D.R. Ecological lessons from Free-Air CO_2 Enrichment (FACE) experiments. *Annu. Rev. Ecol. Evol. Syst.* **42**, 181-203 (2011).
5. Leuzinger S. & Hattenschwiler S. Beyond global change: lessons from 25 years of CO_2 research. *Oecologia* **171,** 639-651 (2013).
6. Arora V.K. *et al.* Carbon-concentration and carbon-climate feedbacks in CMIP5 Earth system models. *J. Clim.* **26**, 5289-5214 (2013).
7. Ellsworth D.S. *et al.* Elevated CO_2 does not increase eucalypt forest productivity on a low-phosphorus soil. *Nat. Clim. Change* **7**, 279-282 (2017).
8. Körner C. *et al.* Carbon flux and growth in mature deciduous forest trees exposed to elevated CO_2. *Science* **309**, 1360-1362 (2005).
9. Ryan M.G. Three decades of research at Flakaliden advancing whole-tree physiology, forest ecosystem and global change research. *Tree Physiol*. **33**, 1123-1131 (2013).
10. Klein T. *et al.* Growth and carbon relations of mature *Picea abies* trees under 5 years of free-air CO_2 enrichment. *J. Ecol.* **104**, 1720-1733 (2016).
11. Norby R.J. *et al.* Model-data synthesis for the next generation of forest free-air CO_2 enrichment (FACE) experiments. *New Phytol.* **209**, 17-28 (2016).

12. Pugh T.A.M. *et al.* Role of forest regrowth in global carbon sink dynamics. *Proc. Natl. Acad. Sci. USA* **116**, 4382-4387 (2019).

13. Grassi G. *et al.* The key role of forests in meeting climate targets requires science for credible mitigation. *Nat. Clim. Change* **7**, 220-226 (2017).

14. Peñuelas J. *et al.* Shifting from a fertilization-dominated to a warming-dominated period. *Nat. Ecol. Evol.* **1**, 1438-1445 (2017).

15. DeLucia E.H. *et al.* Net primary production of a forest ecosystem with experimental CO_2 enrichment. *Science* **285**, 1177-1179 (1999).

16. Medlyn B.E. *et al.* Using models to guide field experiments: a priori predictions for the CO_2 response of a nutrient- and water-limited native Eucalypt woodland. *Global Change Biol.* **22**, 2834-2851 (2016).

17. Medlyn B.E. *et al.* Using ecosystem experiments to improve vegetation models. *Nat. Clim. Change* **5**, 528-534 (2015).

18. Friedlingstein P. *et al*. Uncertainties in CMIP5 climate projections due to carbon cycle feedbacks. *J. Climate* **27**, 511-526 (2014).

19. Yang J. *et al.* Low sensitivity of gross primary production to elevated CO_2 in a mature Eucalypt woodland. *Biogeosci. Discuss*. (submitted).

20. De Lucia E.H. *et al.* Forest carbon use efficiency: is respiration a constant fraction of gross primary production? *Global Change Biol.* **13**, 1157-1167 (2007).

21. Norby R.J. Forest canopy productivity index. *Nature* **381**, 564 (1996).

22. Duursma R.A. *et al*. Canopy leaf area of a mature evergreen Eucalyptus woodland does not respond to elevated atmospheric CO_2 but tracks water availability. *Glob. Chang. Biol*. **22**, 1666-1676 (2016).

616 23. Drake J.E. *et al.* Short-term carbon cycling responses of a mature eucalypt woodland
617 to gradual stepwise enrichment of atmospheric CO_2 concentration. *Glob. Chang. Biol.*
618 **22**, 380-390 (2016).
619 24. Drake J.E. *et al.* Three years of soil respiration in a mature eucalypt woodland exposed
620 to atmospheric CO_2 enrichment. *Biogeochemistry* **139**, 85-101 (2018).
621 25. Drake J.E. *et al.* Increases in the flux of carbon belowground stimulate nitrogen uptake
622 and sustain the long-term enhancement of forest productivity under elevated CO_2. *Ecol.*
623 *Lett*. **14**, 349-357 (2011).
624 26. Hasegawa S. *et al.* Elevated carbon dioxide increases soil nitrogen and phosphorus
625 availability in a phosphorus-limited Eucalyptus woodland. *Global Change Biol.* **22**,
626 1628-1643 (2016).
627 27. Ochoa-Hueso R. *et al.* Rhizosphere-driven increase in nitrogen and phosphorus
628 availability under elevated atmospheric CO_2 in a mature *Eucalyptus* woodland. *Plant*
629 *Soil* **416**, 283-295 (2017).
630 28. Crous K.Y. *et al*. Nitrogen and phosphorus retranslocation of leaves and stemwood in
631 a mature *Eucalyptus* forest exposed to 5 years of elevated CO_2. Front. Plant Sci. **10**:664,
632 doi: 10.3389/fpls.2019.00664 (2019).
633 29. Zaehle S. *et al*. Evaluation of 11 terrestrial carbon-nitrogen cycle models against
634 observations from two temperature Free-Air CO_2 Enrichment studies. *New Phytol.* **202**,
635 803-822 (2014).
636 30. Fleischer K. *et al.* Future CO_2 fertilization of the Amazon forest hinges on plant
637 phosphorus use and acquisition. *Nat. Geosci.* (in press).
638 31. Todd-Brown K.E.O. *et al*. Changes in soil organic carbon storage predicted by earth
639 system models during the 21st century. *Biogeosciences*, **11**, 2341-2356 (2014).

640 32. Kuzyakov Y. *et al.* Review and synthesis of the effects of elevated atmospheric CO_2 on
641 soil processes: no changes in pools, but increased fluxes and accelerated cycles. *Soil*
642 *Biol. Biochem*. **128**, 66-78 (2019).
643 33. Luyssaert S. *et al.* Old-growth forests as global carbon sinks. *Nature* **455**, 213-215
644 (2008).
645 34. Jones C. *et al*. 21st century compatible CO_2 emissions and airborne fraction simulated
646 by CMIP5 Earth System models under 4 representative concentration pathways. *J.*
647 *Clim.* **26**, doi:10.1175–JCLI–D–12–00554.1 (2013).
648 35. Australia Government Department of Agriculture, Fisheries and Forestry. Australia's
649 agriculture, fisheries and forestry at a glance 2012. Canberra, Australia (2012).
650 36. Food and Agricultural Organization of the United Nations. Global Forest Resources
651 Assessment 2000. FAO Forestry Paper 140. Rome, Italy (2001).
652 37. Crous, K. *et al.* Is phosphorus limiting in a mature *Eucalyptus* woodland? Phosphorus
653 fertilization stimulates stem growth. *Plant Soil* **391**, 293-305 (2015).
654 38. Gimeno T.E. *et al.* Elevated CO_2 did not affect the hydrological balance of a mature
655 native *Eucalyptus* woodland. *Glob. Chang. Biol.* **24**, 3010-3024 (2018).
656 39. Hasegawa S. *et al*. Elevated CO_2 concentrations reduce C4 cover and decrease diversity
657 of understorey plant community in a *Eucalyptus* woodland. *J. Ecol.* **106**, 1483–1494
658 (2018).
659 40. Pathare V.S. *et al*. Water availability affects seasonal CO_2-induced photosynthetic
660 enhancement in herbaceous species in a periodically dry woodland. *Glob. Chang. Biol*.
661 **23**, 5164–5178 (2017).
662 41. Paul K.I. *et al.* Development and testing of allometric equations for estimating above-
663 ground biomass of mixed-species environmental plantings. *For. Ecol. Manage.* **310**,
664 483-494 (2013).

42. Collins L. *et al.* Understorey productivity in temperate grassy woodland responds to soil water availability but not to elevated CO_2. *Glob. Chang. Biol*. **24**, 2366-2376 (2018).

43. Snowdon P. *et al.* National carbon accounting system technical report no. 17. Australian Greenhouse Office, Canberra, Australia (2000).

44. Wallander H. *et al.* Evaluation of methods to estimate production, biomass and turnover of ectomycorrhizal mycelium in forests soils – A review. *Soil Biol. biochem.* **57**, 1034–1047 (2013).

45. Buyer J.S. & Sasser M. High throughput phospholipid fatty acid analysis of soils. *Appl. Soil Ecol*. **61**, 127–130 (2012).

46. Gherlenda A.N. *et al*. Boom and bust: rapid feedback responses between insect outbreak dynamics and canopy leaf area impacted by rainfall and CO_2. *Glob. Chang. Biol*. **22**, 3632-3641 (2016).

47. Facey S.L. *et al*. Atmospheric change causes declines in woodland arthropods and impacts specific trophic groups. *Agr. Forest Entomol.* **19**, 101-112 (2017).

48. Trakimas, G. *et al*. Ecological Stoichiometry: a link between developmental speed and physiological stress in an omnivorous insect. *Front. Behav. Neurosci*. **13**:42, https://doi.org/10.3389/fnbeh.2019.00042 (2019).

49. Farquhar G.D. *et al.* A biochemical model of photosynthetic CO_2 assimilation in leaves of C3 species. *Planta* **149**, 78–90 (1980).

50. Gimeno T.E. *et al*. Conserved stomatal behavior under elevated CO_2 and varying water availability in a mature woodland. *Funct. Ecol*. **30**, 700-709 (2016).

51. Medlyn, B.E. *et al.* Reconciling the optimal and empirical approaches to modelling stomatal conductance. *Glob. Chang. Biol*. **17**, 2134–2144 (2011).

689 52. Martins C.S.C. *et al.* Identifying environmental drivers of greenhouse gas emissions
690 under warming and reduced rainfall in boreal-temperate forests. *Funct. Ecol.* **31**, 2356–
691 2368 (2017).
692 53. Reich P.B. *et al.* Plant diversity enhances ecosystem responses to elevated CO_2 and
693 nitrogen deposition. *Nature* **410**, 809-810 (2001).
694 54. Gherlenda A.N. *et al*. Insect herbivory in a mature Eucalyptus woodland canopy
695 depends on leaf phenology but not CO_2 enrichment. *BMC Ecol.* **16**, 47 (2016).
696 55. Gherlenda A.N. *et al*. Precipitation, not CO_2 enrichment, drives insect herbivore frass
697 deposition and subsequent nutrient dynamics in a mature *Eucalyptus* woodland. *Plant*
698 *Soil* **399**, 29-39 (2016).
699 56. Drake J.E. *et al*. The partitioning of gross primary production for young *Eucalyptus*
700 *tereticornis* trees under experimental warming and altered water availability. *New*
701 *Phytol*. **222**, 1298-1312 (2019).
702 57. Salomón R.L. *et al.* Elevated CO_2 does not affect stem CO_2 efflux nor stem respiration
703 in dry Eucalyptus woodland, but it shifts the vertical gradient in xylem CO_2. *Plant Cell*
704 *Environ.* **42**, 2151-2164 (2019).
705 58. Raumonen P. *et al.* Fast Automatic Precision Tree Models from Terrestrial Laser
706 Scanner Data. *Remote Sens.* **5**, 491-520 (2013).
707 59. Calders K. *et al.* Nondestructive estimates of above-ground biomass using terrestrial
708 laser scanning. *Methods Ecol. Evol.* **6**, 198-208 (2015).
709 60. Drake J.E. *et al.* A common thermal niche among geographically diverse populations
710 of the widely distributed tree species Eucalyptus tereticornis: No evidence for
711 adaptation to climate-of-origin. *Glob. Chang. Biol.* **23**, 5069-5082 (2017).
712 61. Drake J.E. *et al.* Does physiological acclimation to climate warming stabilize the ratio
713 of canopy respiration to photosynthesis? *New. Phytol.* **211**, 850-863 (2016).

62. Davidson E.A. *et al*. The Dual Arrhenius and Michaelis–Menten kinetics model for decomposition of soil organic matter at hourly to seasonal time scales. *Glob. Chang. Biol.* **18**, 371-384 (2012).

63. Guenther A.B. *et al.* The Model of Emissions of Gases and Aerosols from Nature version 2.1 (MEGAN2.1): an extended and updated framework for modeling biogenic emissions. *GeoSci. Model Dev*. **5**, 1471-1492 (2012).

64. Emmerson K.M. *et al*. Sensitivity of isoprene emissions to drought over south-eastern Australia: Integrating models and satellite observations of soil moisture, *Atmos. Environ*. **209**, 112-124 (2019).

65. Keith H. *et al*. Multiple measurements constrain estimates of net carbon exchange by a Eucalyptus forest. *Agric. For. Meteorol.* **149**, 535-558 (2009).

66. Bates D. *et al*. Fitting linear mixed-effects models using lme4. *J. Stat. Softw*. **67**, 1-48 (2015).

67. R Core Team. R: A language and environment for statistical computing. R Foundation for Statistical Computing, Vienna, Austria. URL https://www.R-project.org/ (2018).

729 **Acknowledgements**

730 EucFACE was built as an initiative of the Australian Government as part of the Nation-building
731 Economic Stimulus Package, and is supported by the Australian Commonwealth in
732 collaboration with Western Sydney University. We acknowledge the technical support by V.
733 Kumar and C. McNamara, and the team of people who have assisted with data collection. The
734 Eucalyptus tree vector in Figure 1 is from Heydon, L. *Eucalyptus spp*. Integration and
735 Application Network, University of Maryland Center for Environmental Science
736 (ian.umces.edu/imagelibrary/). This work was partially supported by the following grants from
737 the Australian Research Council: DP130102501 (to JRP and ICA), DP110105102 and
738 DP160102452 (to DSE). RLS received funding from Research Foundation Flanders and the
739 European Union's Horizon 2020 research and innovation programme under the Marie
740 Skłodowska- Curie grant agreement no. 665501. RO-H. is financially supported by a Ramón
741 y Cajal Fellowship from MICIU (RYC-2017-22032).

742

743 **Author contributions**

744 MJ, BEM, RAD and JED designed the synthesis, compiled the data, and performed the
745 analyses. MJ, BEM, RAD, JED, ICA, CVMB, MMB, LC-G, YC, LC, KYC, SLF, ANG, TEG,
746 SH, SNJ, CAM, KM, BDM, LN, UNN, NJN, RO-H, VSP, EP, JP, JRP, SAP, PBR, AAR, MR,
747 PR, RLS, BKS, BS, MGT, JKMW, AW-K, JY and DSE collected data and contributed to data
748 analyses. JY and BEM performed the MAESPA model simulations, with contributions from
749 MGDK and RAD. JED and AAR performed soil respiration gap-filling and modelling. KME
750 performed isoprene emission model simulation. MJ and LC-G conceptualized Figure 1, and
751 LC-G implemented the graphic design. MJ wrote the initial manuscript, with significant input

752 from BEM, JED, BS, PBR, SZ, MGDK, MGT and DSE. All authors edited and approved the
753 manuscript.
754

755 **Competing financial interests**

756 None declared.
757

758 **Materials and Correspondence**

759 Correspondence should be directed to MJ (m.jiang@westernsydney.edu.au) and BEM
760 (b.medlyn@westernsydney.edu.au).

761 **Figures**

762

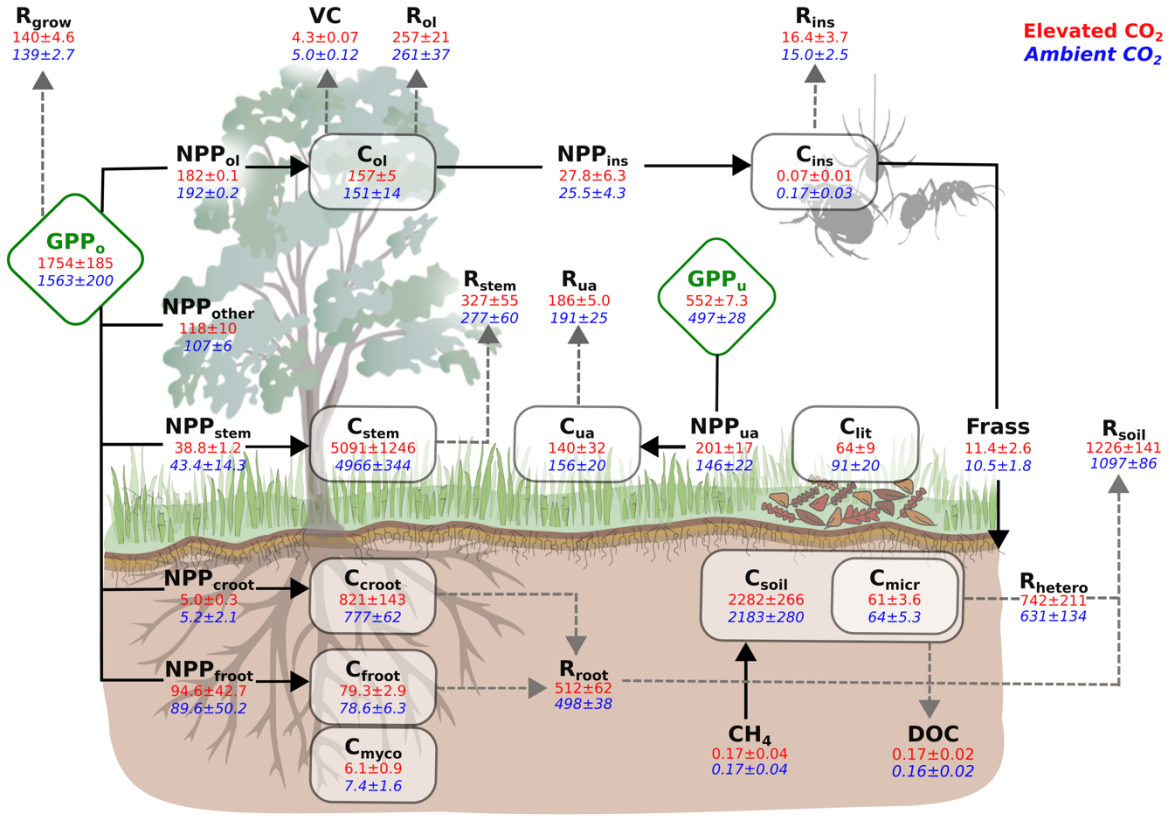

763

764 **Figure 1. A comprehensive carbon budget under ambient and elevated CO_2 treatment in**
765 **a mature forest ecosystem.** Diamond boxes are gross primary production for overstorey
766 (GPP_o) and understorey (GPP_u), respectively. Squared boxes are carbon stocks (gCm^{-2}),
767 including overstorey leaf (C_{ol}), stem (C_{stem}), coarse root (C_{croot}), fineroot (C_{froot}), understorey
768 aboveground (C_{ua}), leaf litter (C_{lit}), soil (C_{soil}), microbe (C_{micr}), aboveground insect (C_{ins}), and
769 mycorrhizae (C_{myco}). Unboxed variables are carbon fluxes ($gCm^{-2}yr^{-1}$), including net primary
770 production of overstorey leaf (NPP_{ol}), stem (NPP_{stem}), coarse root (NPP_{croot}), fineroot (NPP_{froot}),
771 and understorey aboveground (NPP_{ua}), overstorey leaf consumption by insects (NPP_{ins}),
772 respiration fluxes of overstorey leaf (R_{ol}), stem (R_{stem}), root (R_{root}), understorey aboveground
773 (R_{ua}), growth (R_{grow}), insect (R_{ins}), heterotroph (R_{hetero}), and soil (R_{soil}), and volatile carbon
774 emission (VC), frass production (Frass), dissolved organic carbon (DOC), and soil methane net

775 uptake (CH_4). Solid arrow lines are fluxes entering a pool, dotted arrow lines are fluxes leaving
776 a pool. Blue italic values are means ± one standard deviation of the ambient CO_2 treatment
777 (n=3), whereas red values are means ± one standard deviation of the elevated CO_2 treatment
778 (n=3). All values are normalized by a linear mixed-model with plot-specific pre-treatment leaf
779 area index as a covariate to account for pre-existing differences. Summary of variable
780 definitions and data availability is provided in Extended Data Table 1.

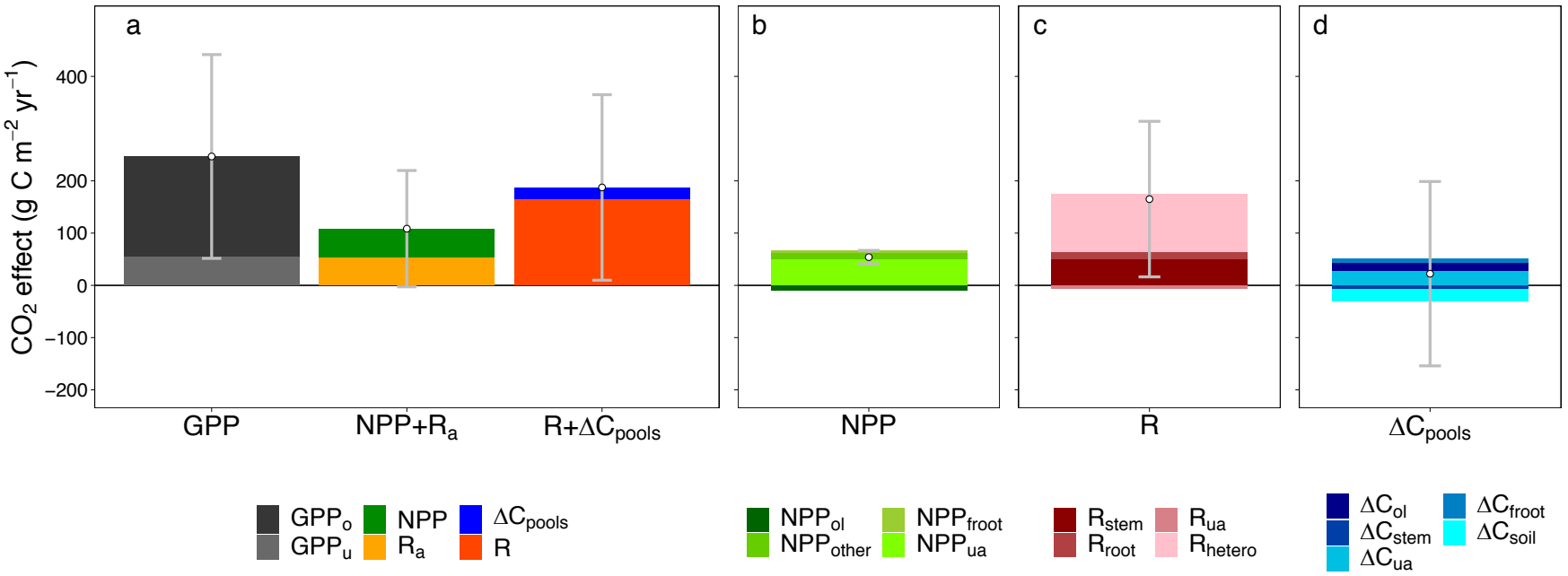

Figure 2. The fate of additional carbon fixed under elevated CO_2 (eCO_2) in a mature forest ecosystem. a) Column **"**GPP" represents the total eCO_2-induced increases in overstorey and understorey gross primary production (GPP_o and GPP_u, respectively), "NPP + R_a" represents the sum of net primary production and autotrophic respiration response, "R + ΔC_{pools}" represents the sum of ecosystem respiration and carbon storage response. **b)** The relative contributions of individual NPP fluxes to the aggregated NPP response to eCO_2, including NPP responses of overstorey leaf (NPP_{ol}), twigs, barks and seeds (NPP_{other}), fineroot (NPP_{froot}), and understorey aboveground (NPP_{ua}); **c)** The relative contributions of individual respiratory fluxes to the aggregated R response to eCO_2, including respiration responses of stem (R_{stem}), root (R_{root}), understorey aboveground

789 (R_{ua}), and soil heterotroph (R_{hetero}); and **d)** The relative contributions of individual change in carbon storage to the aggregated ΔC_{pools} response to
790 eCO_2, including changes in pool of overstorey leaf (ΔC_{ol}), stem (ΔC_{stem}), understorey aboveground (ΔC_{ua}), fineroot (ΔC_{froot}), and soil (ΔC_{soil}).
791 Variables with an absolute mean CO_2 effect of < 5 $gCm^{-2}yr^{-1}$ are excluded from the figure for better visual clarification. Individual CO_2 responses
792 are reported in Extended Data Figure 4. Each color represents the CO_2 response of a flux variable, point indicates the net sum of all variables for
793 a column, and the grey error bar represents one standard deviation of the estimated column sum at the plot-level (see Methods). The CO_2 effect is
794 estimated using a linear mixed-model analysis with plot-specific pre-treatment leaf area index as a covariate to account for pre-existing differences
795 (see Methods). The un-normalized response is provided in Extended Data Figure 3, which generally agrees with findings present in this figure, but
796 with less statistical precision.

797

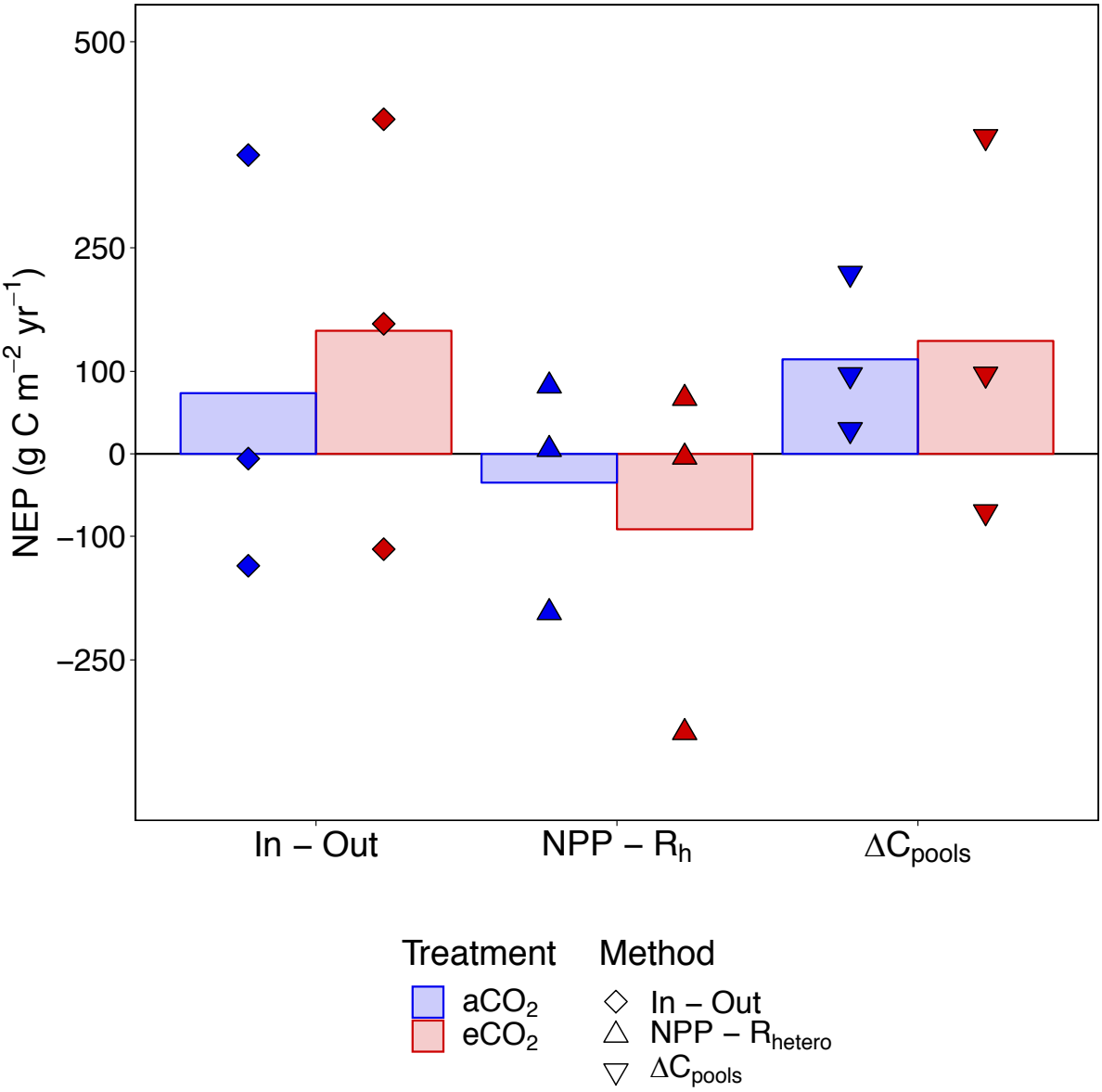

798

799 **Figure 3. Estimates of net ecosystem production (NEP) under ambient and elevated CO_2**
800 **treatment at EucFACE**. Positive values indicate ecosystem net carbon uptake by the
801 ecosystem. "In - Out" calculates NEP based on the difference between total influxes and total
802 outfluxes. "NPP - R_{hetero}" calculates NEP based on the difference between net primary
803 production (NPP) and heterotrophic respiration (R_{hetero}). "ΔC_{pools}" derives NEP based on
804 incremental changes in all ecosystem carbon pools. Colored bars indicate treatment means
805 based on each method (n=3), with blue representing ambient and red representing elevated CO_2

806 treatment. Individual dots are plot-level NEP, derived based on different methods (see
807 Methods). Values are normalized by a linear mixed-model with plot-specific pre-treatment leaf
808 area index as a covariate to account for pre-existing differences. Horizontal dotted line indicates
809 NEP equals zero.

Extended Data Table 1. Definition and data availability of variables. Data availability includes start and end year of data included in this study. Time points indicate the number of data collections over the available data period. Within plot sub-replicate indicate the number of replicates within each treatment plot. The detailed methods for estimating each variable is provided in the Method section.

Variable		Data coverage			
Name	**Symbol**	**Start year**	**End year**	**Time points**	**Within plot sub-replicate ($plot^{-1}$)**
Specific Leaf Area	SLA	2013	2016	50	3
Leaf Area Index	LAI	2012	2016	303	1
Soil bulk density	BK	2017	2017	2	3
Diameter at breast height	DBH	2013	2016	4	Individual tree
Overstorey leaf pool	C_{ol}	2012	2016	303	1
Understorey aboveground pool	C_{ua}	2015	2016	16	4
Overstorey stem C pool	C_{stem}	2013	2016	4	Individual tree
Fine root C pool	C_{froot}	2014	2016	6	4
Coarse root C pool	C_{croot}	2013	2016	4	Individual tree
Forest floor leaf litter C pool	C_{lit}	2013	2016	46	-
Microbial C pool	C_{micr}	2012	2015	15	4
Soil C pool	C_{soil}	2012	2014	11	4

Mycorrhizal C pool	C_{myco}	2015	2015	3	-
Insect C pool (aeriel)	C_{ins}	2013	2016	43	8
Insect C pool (ground dwelling)	C_{ins}	2013	2015	5	4
Overstorey gross primary production	GPP_o	2013	2016	Annual	1
Understorey gross primary production	GPP_u	2013	2016	Annual	1
Overstorey leaf respiration	R_{ol}	2013	2016	Annual	1
Understorey leaf respiration	R_{ua}	2013	2016	Annual	1
Stem respiration	R_{stem}	2012	2016	Daily	3
Root respiration	R_{root}	2012	2015	Daily	-
Methane net flux	CH_4	2013	2016	35	7
Volatile C emission flux	VC	2013	2016	Daily	1
Insect herbivore respiration	R_{ins}	2012	2014	22	-
Dissolved organic C loss flux	DOC	2012	2014	12	4
Soil respiration	R_{soil}	2012	2015	Daily	8
Growth respiration	R_{grow}	2012	2016	Annual	1
Overstorey leaf net primary production	NPP_{ol}	2012	2016	49	8
Stem net primary production	NPP_{stem}	2012	2016	4	Individual tree

Fine root net primary production	NPP_{froot}	2014	2016	5	4
Coarse root net primary production	NPP_{croot}	2012	2016	4	Individual tree
Other net primary production (sum of twigs, bark, seeds)	NPP_{other}	2012	2016	49	8
Twig net primary production	NPP_{twig}	2012	2016	49	8
Bark net primary production	NPP_{bark}	2012	2016	49	8
Seed net primary production	NPP_{seed}	2012	2016	49	8
Understorey aboveground net primary production	NPP_{ua}	2015	2016	3	4
Frass production	Frass	2012	2014	22	8
Heterotrophic respiration	R_{hetero}	2012	2016	Daily	8
Overstorey leaf insect consumption flux	NPP_{ins}	2012	2014	22	-

815

816 **Extended Data Table 2. Carbon (C) fraction used to convert from biomass into C content.**

Variable	Symbol	Mean value	Data source
C fraction of overstorey leaf pool	f_{ol}	0.5	EucFACE data
C fraction of understorey aboveground pool	f_{ua}	0.456	EucFACE data
C fraction of stem pool	f_{stem}	0.445 (ambient plots) 0.448 (elevated plots)	EucFACE data
C fraction of coarse root pool	f_{croot}	0.445 (ambient plots) 0.448 (elevated plots)	Assumed the same as f_{stem}
C fraction of fine root pool	f_{froot}	0.40 (ambient plots) 0.42 (elevated plots)	EucFACE data
C fraction of overstorey leaflitter pool	f_{lit}	0.5	EucFACE data
C fraction of aboveground insect pool	f_{ins}	0.5	Ref 48
C fraction of frass production	f_{frass}	0.53	EucFACE data
C fraction of microbial pool	f_{micr}	0.534 (ambient plots) 0.493 (elevated plots)	EucFACE data

C fraction of mycorrhizal pool	f_{myco}	0.534 (ambient plots) 0.493 (elevated plots)	Assumed the same as f_{micr}
C fraction of soil pool	f_{soil}	0.016 (ambient plots) 0.017 (elevated plots)	EucFACE data
C fraction of twigs, barks and seeds production	f_{other}	0.5	Assumed

817

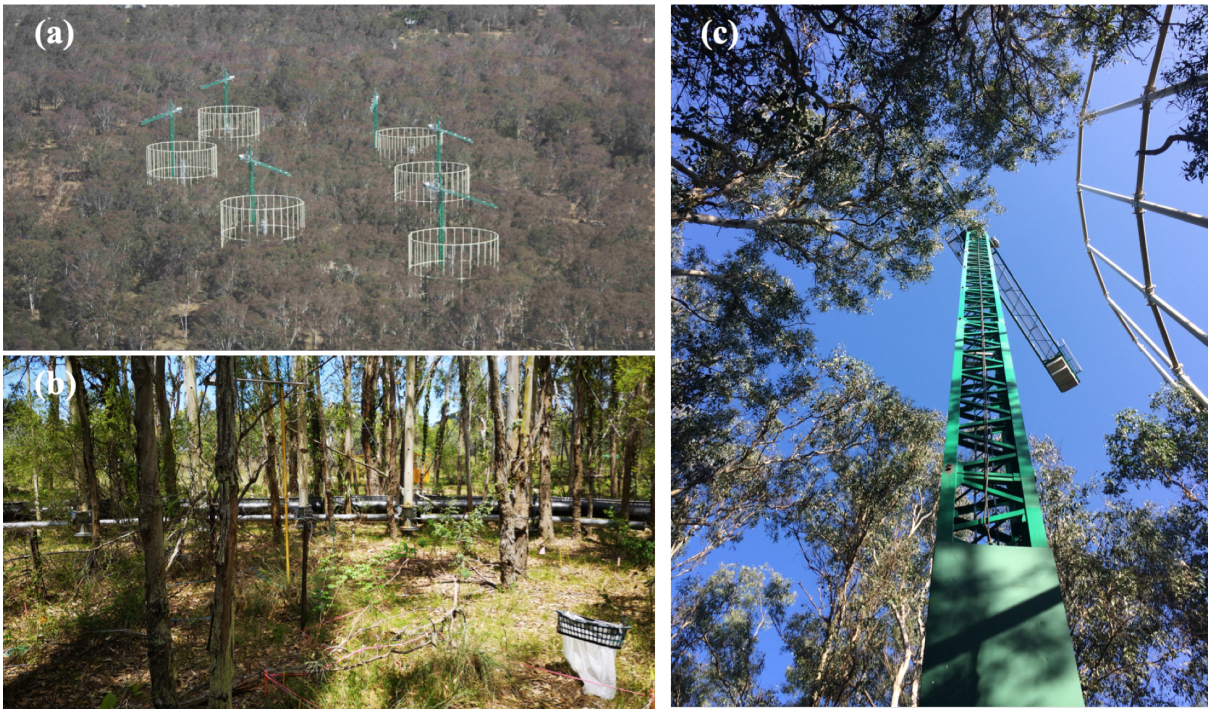

818

819 **Extended Data Figure 1. The *Eucalyptus* free air carbon dioxide enrichment experiment**

820 **facility (EucFACE)**. **a)** A spatial overview of the forest and the facility (photo credit: David

821 S. Ellsworth), **b)** an overview of the understorey vegetation and infrastructure inside a plot

822 (photo credit: Mingkai Jiang), and **c)** a bottom-up look of the canopy structure and the crane

823 (photo credit: Mingkai Jiang).

824

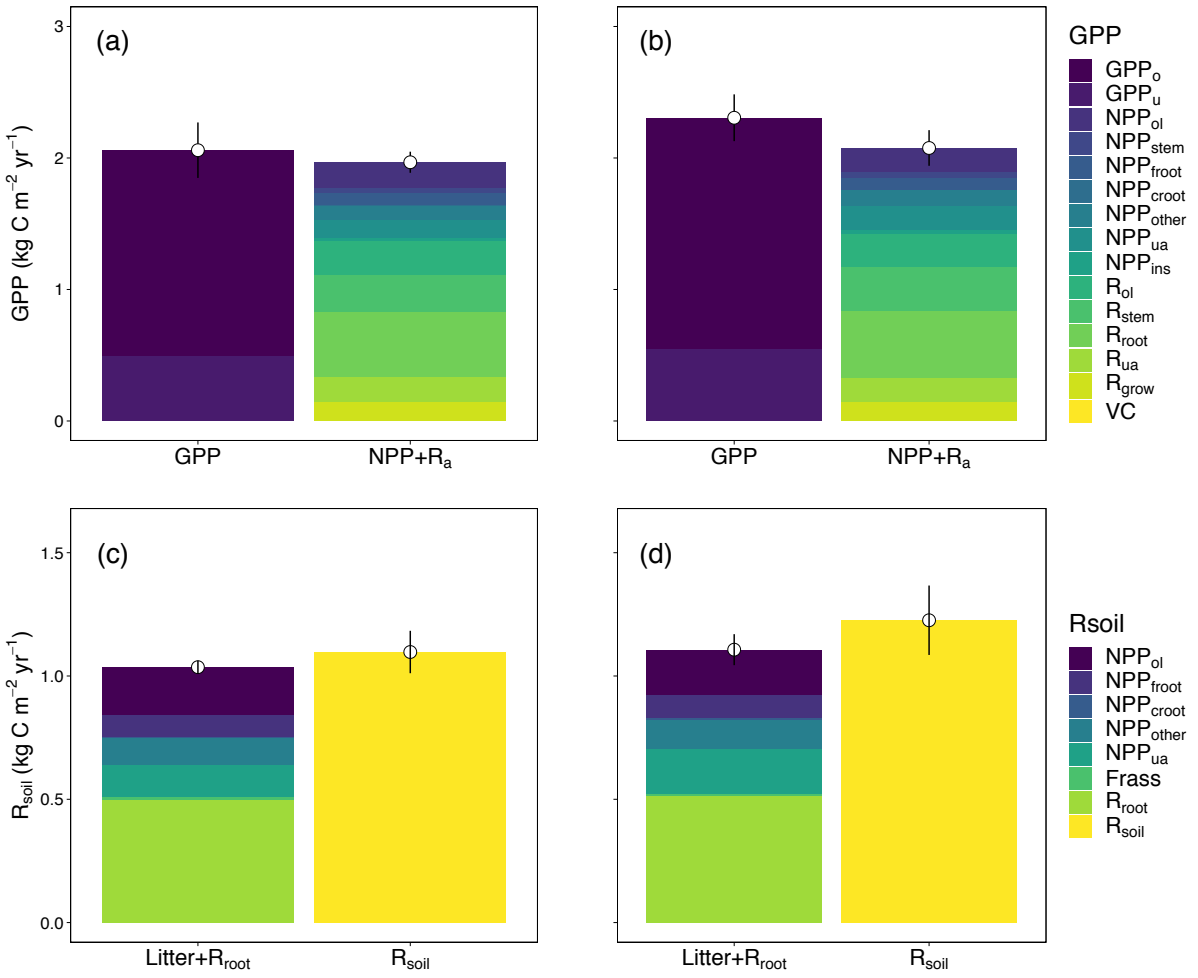

Extended Data Figure 2. Estimates of (a and b) gross primary production (GPP) and (c and d) soil respiration (R_{soil}) based on different methods for both (a and c) ambient and (b and d) elevated CO_2 treatment at EucFACE. For estimates of GPP, we compared the model simulated total GPP of overstorey and understorey (GPP_o and GPP_u, respectively), with the sum of data-driven estimates of net primary production (NPP) and autotrophic respiration (R_a), which include NPP of overstorey leaf (NPP_{ol}), stem (NPP_{stem}), fineroot (NPP_{froot}), coarse root (NPP_{croot}), twigs, barks and seeds (NPP_{other}), understorey aboveground (NPP_{ua}), leaf consumption by insects (NPP_{ins}), and respiratory fluxes of overstorey leaf (R_{ol}), stem (R_{stem}), root (R_{root}), understorey aboveground (R_{ua}), growth (R_{grow}), and volatile carbon emission (VC). For estimates of R_{soil}, we compared direct estimates of R_{soil} scaled up from soil chamber

measurements, with the sum of litterfall and independent estimates of root respiration (Litter + R_{root}), assuming no net change in soil carbon stock over time. Here litterfall was inferred based on NPP of overstorey leaf (NPP_{ol}), fineroot (NPP_{froot}), coarse root (NPP_{croot}), twigs, barks and seeds (NPP_{other}), understorey aboveground (NPP_{ua}), and frass production (Frass). These evaluations provide independent mass balance checks of the estimated ecosystem carbon budget. Each color represents a flux variable. Dotted point and vertical line represent treatment mean and standard deviation based on plot-level estimates of the aggregated flux (n=3). Values were normalized by a linear mixed-model with pre-treatment leaf area index as a covariate to account for pre-existing differences.

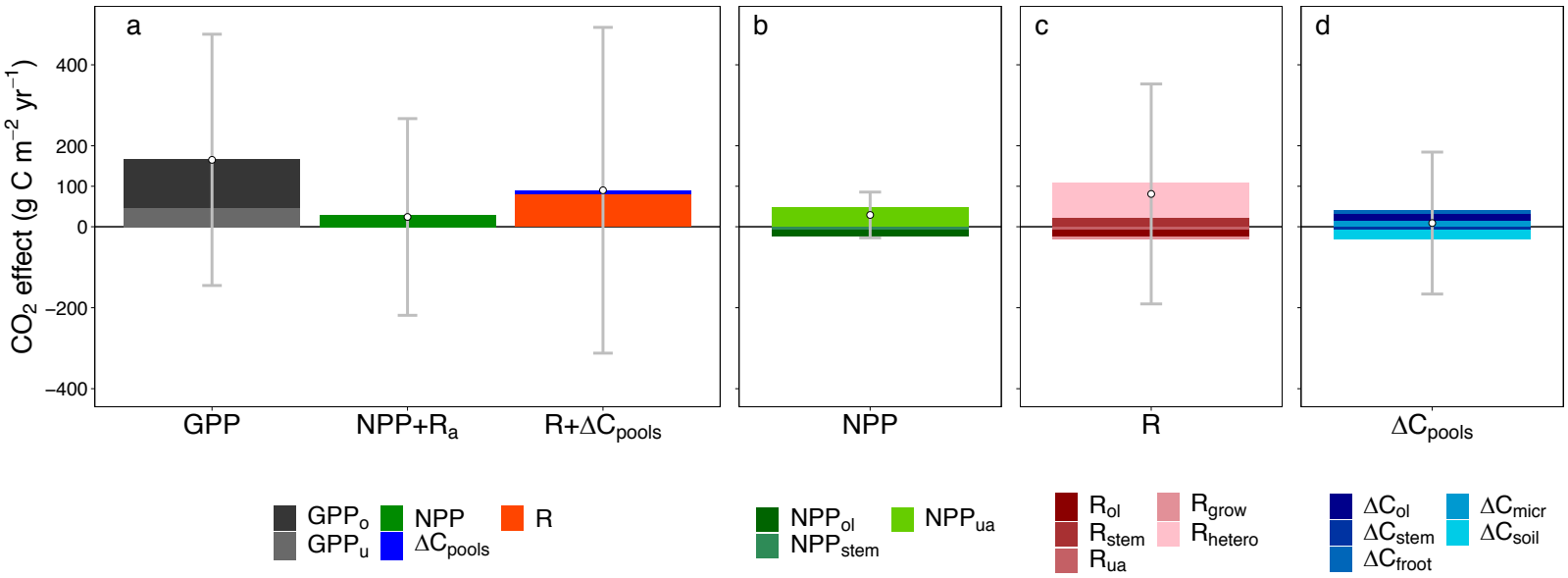

Extended Data Figure 3. The fate of additional carbon fixed under elevated CO_2 (eCO_2) in a mature forest ecosystem (non-normalized analysis case). a) Column **"**GPP" represents the total eCO_2 induced increase in overstorey and understorey gross primary production (GPP_o and GPP_u, respectively), column "NPP + R_a" represents the sum of net primary production and autotrophic respiration eCO_2 response, and column "R + ΔC_{pools}" represents the sum of ecosystem respiration and carbon storage eCO_2 response. **b)** The relative contributions of individual NPP fluxes to the aggregated NPP response to eCO_2, including overstorey leaf (NPP_{ol}), stem (NPP_{stem}), and understorey aboveground (NPP_{ua}). **c)** The relative contributions of individual respiratory fluxes to the aggregated R response to eCO_2, including overstorey leaf (R_{ol}), stem (R_{stem}), understorey aboveground (R_{ua}), growth (R_{grow}), and heterotroph (R_{hetero}). **d)** The relative contributions of individual change in carbon storage to the aggregated ΔC_{pools} response to eCO_2, including overstorey leaf (ΔC_{ol}), stem (ΔC_{stem}), fineroot (ΔC_{froot}), microbe (ΔC_{micr}), and soil (ΔC_{soil}). Variables with an

855 average CO_2 effect of < 5 $gCm^{-2}yr^{-1}$ were excluded from the figure for better visual clarification. Each color represents a flux variable, point
856 indicates the net sum of all variables for a column, and the grey confidence interval represents plot-level standard deviation (n=3) of the estimated
857 column sum.

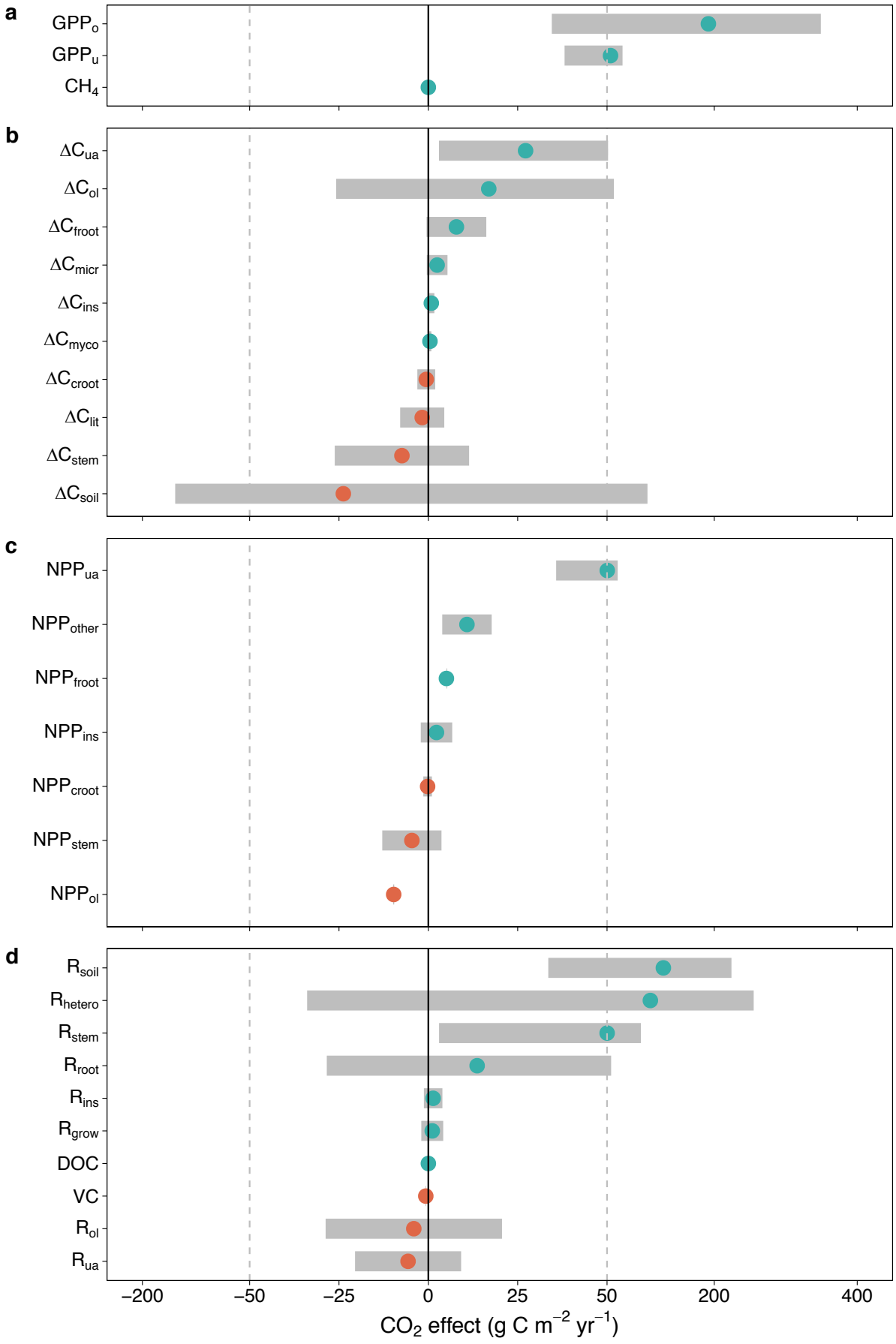

858

Extended Data Figure 4. CO_2 treatment effect ($gCm^{-2}yr^{-1}$) for all ecosystem fluxes at EucFACE. a) The CO_2 response of gross ecosystem carbon uptake, including gross primary production of overstorey (GPP_o) and understorey (GPP_u), and soil methane uptake (CH_4). **b)** The eCO_2 response of annual incremental change in carbon pool (ΔC_{pools}), including overstorey leaf (ΔC_{ol}), stem (ΔC_{stem}), coarse root (ΔC_{croot}), fineroot (ΔC_{froot}), understorey aboveground (ΔC_{ua}), leaf litter (ΔC_{lit}), soil (ΔC_{soil}), microbe (ΔC_{micr}), aboveground insect (ΔC_{ins}), and mycorrhizae (ΔC_{myco}). **c)** The eCO_2 response of net primary production (NPP), including overstorey leaf (NPP_{ol}), stem (NPP_{stem}), coarse root (NPP_{croot}), fineroot (NPP_{froot}), understorey aboveground (NPP_{ua}), twigs, barks and seeds (NPP_{other}), and leaf insect consumption (NPP_{ins}). **d)** The eCO_2 response of ecosystem respiration (R) and other out-going flux, including respiration fluxes of overstorey leaf (R_{ol}), stem (R_{stem}), root (R_{root}), understorey aboveground (R_{ua}), growth (R_{grow}), insect (R_{ins}), heterotroph (R_{hetero}), and soil (R_{soil}), and volatile carbon emission (VC) and dissolved organic carbon leaching (DOC). Dots and grey bars represent means and standard deviations of the CO_2 treatment difference, predicted by a linear mixed-model with plot-specific pre-treatment leaf area index as a covariate. Orange dots indicate negative means and light green dots indicate positive means. Dashed lines indicate change of scale along the x-axis.